Summer 8-28-2019

Emergence of tissue-like mechanics from fibrous networks confined by close-packed cells

Anne van Oosten
University of Pennsylvania

Xingyu Chen
University of Pennsylvania

LiKang Chin
University of Pennsylvania

Katrina Cruz
University of Pennsylvania

Alison E. Patteson
University of Pennsylvania, Syracuse University

See next page for additional authors

Recommended Citation

van Oosten, A.S.G., Chen, X., Chin, L. et al. Emergence of tissue-like mechanics from fibrous networks confined by close-packed cells. Nature 573, 96–101 (2019). https://doi.org/10.1038/s41586-019-1516-5

LETTER

https://doi.org/10.1038/s41586-019-1516-5

Emergence of tissue-like mechanics from fibrous networks confined by close-packed cells

Anne S. G. van Oosten[1,2,8,9], Xingyu Chen[2,3,9], LiKang Chin[1,2], Katrina Cruz[1,2], Alison E. Patteson[1,2,4], Katarzyna Pogoda[1,2,5], Vivek B. Shenoy[2,3]* & Paul A. Janmey[1,2,6,7]*

The viscoelasticity of the crosslinked semiflexible polymer networks—such as the internal cytoskeleton and the extracellular matrix—that provide shape and mechanical resistance against deformation is assumed to dominate tissue mechanics. However, the mechanical responses of soft tissues and semiflexible polymer gels differ in many respects. Tissues stiffen in compression but not in extension[1–5], whereas semiflexible polymer networks soften in compression and stiffen in extension[6,7]. In shear deformation, semiflexible polymer gels stiffen with increasing strain, but tissues do not[1–8]. Here we use multiple experimental systems and a theoretical model to show that a combination of nonlinear polymer network elasticity and particle (cell) inclusions is essential to mimic tissue mechanics that cannot be reproduced by either biopolymer networks or colloidal particle systems alone. Tissue rheology emerges from an interplay between strain-stiffening polymer networks and volume-conserving cells within them. Polymer networks that soften in compression but stiffen in extension can be converted to materials that stiffen in compression but not in extension by including within the network either cells or inert particles to restrict the relaxation modes of the fibrous networks that surround them. Particle inclusions also suppress stiffening in shear deformation; when the particle volume fraction is low, they have little effect on the elasticity of the polymer networks. However, as the particles become more closely packed, the material switches from compression softening to compression stiffening. The emergence of an elastic response in these composite materials has implications for how tissue stiffness is altered in disease and can lead to cellular dysfunction[9–11]. Additionally, the findings could be used in the design of biomaterials with physiologically relevant mechanical properties.

Figure 1 and Supplementary Fig. 1 show that adipose, kidney, liver, lung and spinal cord tissue stiffens in compression and remains constant or softens in extension, whereas gels formed by crosslinked biopolymers such as collagen (or fibrin[6,7]) soften in compression and stiffen in extension (Fig. 1b). Additionally, collagen and other fibrous biopolymer networks show strong shear strain stiffening, whereas tissues show gradual shear strain softening (Fig. 1c). The difference between soft tissues and biopolymer networks cannot be explained by differences in fluid permeability; replacing aqueous buffer with long, hygroscopic hyaluronic acid polymers increases viscosity (Supplementary Fig. 2) but does not prevent compression softening (Fig. 1b).

One hypothesis for the difference between tissues and pure polymer networks is that in tissues the polymer networks that form the cytoskeleton and the extracellular matrix (ECM) are under tension generated by motor proteins. This hypothesis was tested by comparing gels formed by purified fibrin—the polymer network within blood clots—with clots formed by whole blood, in which platelets pre-stress the fibrin network around red blood cells (RBCs). Whole blood clots have shear storage moduli comparable to those of adipose tissue, and shear strain stiffening is largely abolished (Fig. 1c), as was previously observed by comparing platelet-poor and platelet-rich plasma clots[7,8]. However, unlike tissues, plasma clots soften when compressed, suggesting that tension alone does not account for tissue-like rheology.

In addition to fibrin networks, blood clots also contain RBCs at the volume fraction of the haematocrit (about 40%) within the network, whereas purified biopolymer networks contain only fluid. To test whether particle inclusion alone, or in combination with polymer prestress, could account for the compression stiffening of tissues, whole blood was clotted between rheometer plates held initially at constant separation, allowing platelets to stress the fibrin network, but preventing volume change due to expulsion of serum. Platelet contractility was in some cases prevented by adding a myosin inhibitor.

Without any axial tension or compression, whole blood clots (Fig. 1d) are stiffer than blebbistatin-treated clots (Fig. 1e) and fibrin networks (Fig. 1f). Although the fibrin network structures are slightly different in the three samples (Supplementary Fig. 3), they all soften in compression and stiffen in extension. In native whole clots the effect is symmetric in compression and extension and smaller than in fibrin and blebbistatin-treated clots, which show a different slope between compression and extension (Supplementary Fig. 4). The loss tangent—a measure of viscous dissipation—is small and increases slightly in compression (Supplementary Fig. 5). Blebbistatin treatment restores shear strain stiffening in whole clots (Fig. 1g), but neither native nor platelet-inhibited blood clots stiffen under compression as tissues do. The effect of RBCs at this density is small. The rheology of whole blood clots and plasma clots, with (Supplementary Fig. 6a) and without (Supplementary Fig. 6b) active platelets, is strikingly similar.

At the density of RBCs in blood, neither contractile forces nor particle inclusions account for the differences between polymer networks such as the ECM and whole tissue. Therefore, the effect of a high cell volume fraction was closely investigated by allowing blood to clot without restraining its shape, thereby increasing RBC density as the contracting clot expels serum and forms disk-shaped clots with little (if any) fluid between tightly packed RBCs enwrapped by fibrin (histology of contracted clot in Supplementary Fig. 7b). The compression stiffening and extension weakening observed in soft tissue (Figs. 1b, 2a, Supplementary Fig. 1; histology of adipose in Supplementary Fig. 7a) are also seen in contracted blood clots (Fig. 2c). By contrast, concanavalin A-agglutinated RBCs (Fig. 2c), as well as pellets of tightly packed NIH3T3 fibroblasts (Fig. 2b; imaging in Supplementary Fig. 7c), have much lower shear storage moduli than blood clots and modest compression stiffening. These four materials are compared in Supplementary Fig. 8. Overall these results suggest that tight cell packing is necessary, but not sufficient, for the mechanical footprint of tissues. Loss moduli of the samples vary, but show a

[1]Institute for Medicine and Engineering, University of Pennsylvania, Philadelphia, PA, USA. [2]Center for Engineering Mechanobiology, University of Pennsylvania, Philadelphia, PA, USA. [3]Department of Materials Science and Engineering, University of Pennsylvania, Philadelphia, PA, USA. [4]Department of Physics, Syracuse University, Syracuse, NY, USA. [5]Institute of Nuclear Physics, Polish Academy of Sciences, PL-31342, Krakow, Poland. [6]Department of Physiology, University of Pennsylvania, Philadelphia, PA, USA. [7]Department of Physics, University of Pennsylvania, Philadelphia, PA, USA. [8]Present address: Leiden Academic Centre for Drug Research, Leiden University, Leiden, The Netherlands. [9]These authors contributed equally: Anne S. G. van Oosten, Xingyu Chen. *e-mail: vshenoy@seas.upenn.edu; janmey@pennmedicine.upenn.edu

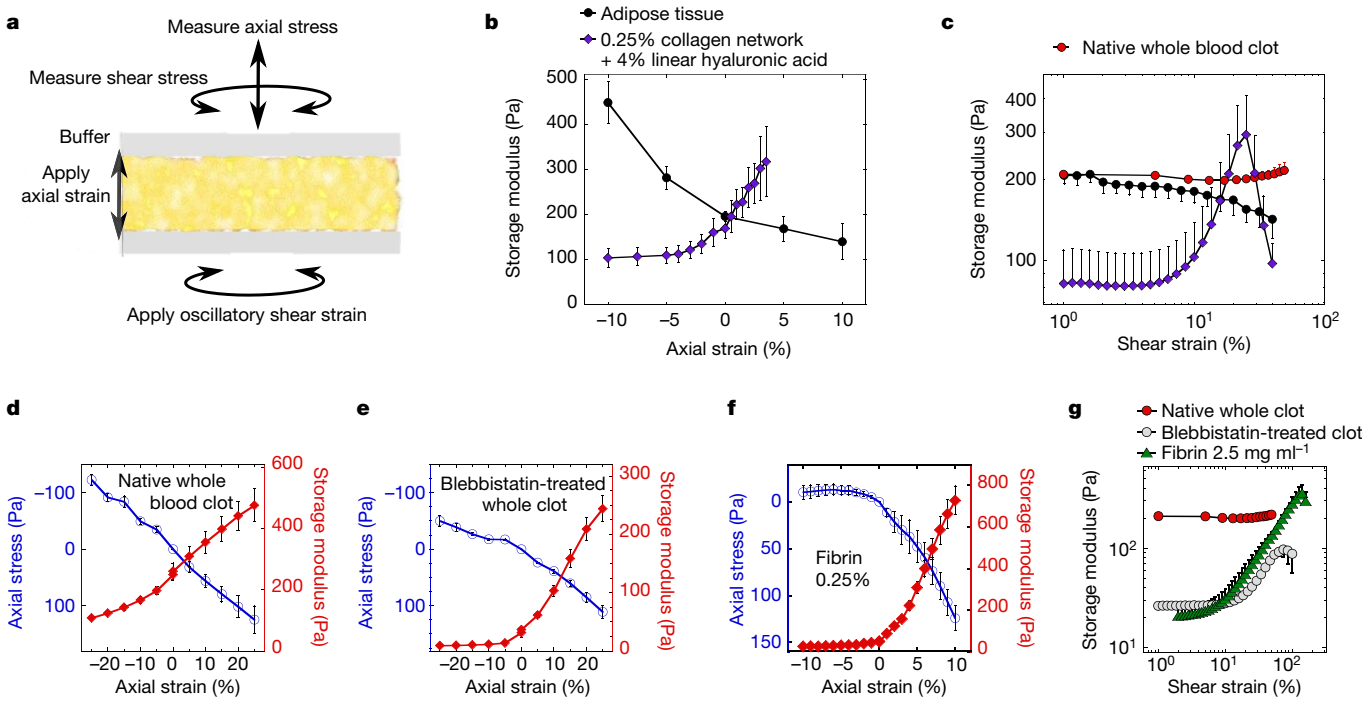

Fig. 1 | Multiaxial rheological behaviour of adipose tissue, reconstituted ECM networks and blood clots. a, A parallel-plate strain-controlled, rotational shear rheometer is used to apply oscillatory shear strain by rotating the bottom plate. Axial strain is applied by step-wise changing the gap height between the plates. The upper plate is attached to a force sensor to measure the torque (shear stress) and the axial stress. **b**, Shear storage modulus measured at 1%–2% shear strain as a function of axial strain for adipose tissue and for a 0.25% collagen network filled with a viscous, linear hyaluronic acid solution of 4%. **c**, Dependence on the shear strain amplitude for adipose tissue (black circles), collagen + hyaluronic acid (black diamonds) and native whole blood clots (red circles). For clarity, one-sided error bars (one standard error) are used. **d**–**f**, Axial stress and shear storage modulus as a function of axial strain of native whole blood clots (**d**), blebbistatin-treated whole blood clots (**e**) and reconstituted fibrin networks (**f**). **g**, Dependence on shear strain amplitude for whole clots, fibrin and blebbistatin-treated clots. For blood the data shown are means of four biological replicates and for the other samples they are means of three biological replicates; error bars show one standard error. Negative axial strain denotes compression and positive axial strain represents extension. The axial stress of fibrin networks was measured with an Instron tensile tester with parallel plates.

downward trend in compression (Supplementary Fig. 9). With respect to shear deformation, adipose tissue shows mild softening at increasing strains (Fig. 2d). Both contracted clots and agglutinated RBCs show considerable shear strain softening after a critical shear strain value is reached, and NIH3T3 cell pellets soften over the whole range of tested shear strains (Fig. 2d).

To produce a cell–gel system that more closely resembles a tissue, mouse embryo fibroblasts (Fig. 2e) and two glioma cell lines, LN229 and LBC3 (Fig. 2f, imaging in Supplementary Fig. 10a), were encapsulated within a collagen gel and allowed to remodel the system by proliferating and contracting the collagen network for seven days. On day 1, when cells had contracted the gel, but had not substantially proliferated, and occupied less than 10% of the volume, the gel–cell composite did not stiffen in compression of up to 20%. After seven days, when cell proliferation and network remodelling had increased cell density, the sample switched to compression stiffening, similar to that seen in spinal cord or brain[3] (Supplementary Fig. 1d). The importance of cells within intact tissues was tested by their gradual removal from liver and brain. Decellularization did not alter the shear modulus of either tissue when measured without compression (Supplementary Fig. 11), consistent with a dominant role of the ECM, but strongly reduced the degree of compression stiffening (Fig. 2g, h).

To determine whether particle packing within an ECM but without cell-generated force can mimic tissue mechanics, fibrin networks were polymerized around various volume fractions of two types of particles: dextran beads, which do not bind proteins, and sulfopropyl-modified dextran beads, which bind fibrinogen. The fibrin network does not infiltrate the particles, and the particles are larger than the mesh size of the network (Supplementary Fig. 12). Because the fibrin network is more permeable than the dextran bead, fluid flows from the network into the surrounding reservoir during compression (increasing bead density) and into the network during extension (decreasing bead density). Fibrin with 50% inert beads initially softens in compression, like the fibrin network alone does, but after 10% compression as the bead density increases, the trend reverses with the storage modulus and nearly doubles after 20% compression (Fig. 3a). With an initial bead density of 60%, no softening occurs with compression and the storage modulus increases 6.3 times (Fig. 3c). In extension, stiffening is less than for fibrin networks without beads or blebbistatin-treated whole clots (Fig. 1). Fibrin networks with high volume fractions of RBCs show similar compression stiffening (Supplementary Fig. 13). When the beads adhere to the fibrin network, compression stiffening is similar to that of fibrin gels with inert beads but occurs at a lower volume fraction (Fig. 3b). In this case, 17% adherent beads suppress compression softening of fibrin (Fig. 3c) and 35% adherent beads stiffen the composite as much as 60% inert beads do (Fig. 3c). The shear-strain-stiffening behaviour of fibrin is also decreased by densely packed beads (Supplementary Fig. 16).

Tissue-like compression stiffening requires embedding particles in a nonlinear strain-stiffening network because beads embedded in a linear elastic polyacrylamide (PAA) gel do not increase the shear modulus with compression (Fig. 3d). At these densities, the compression stiffening was an order or magnitude lower than that for fibrin with 60% inert beads or 35% adherent beads.

Combining volume-conserving beads with contractile cells enhances compression stiffening. Figure 3e shows how a low volume fraction (<10%) of fibroblasts increases the stiffening effects of 14% adherent beads within a fibrin network. The network by itself softens in compression and the beads alone suppress softening but do not produce stiffening in compression (Fig. 3e). However, when the cells contract

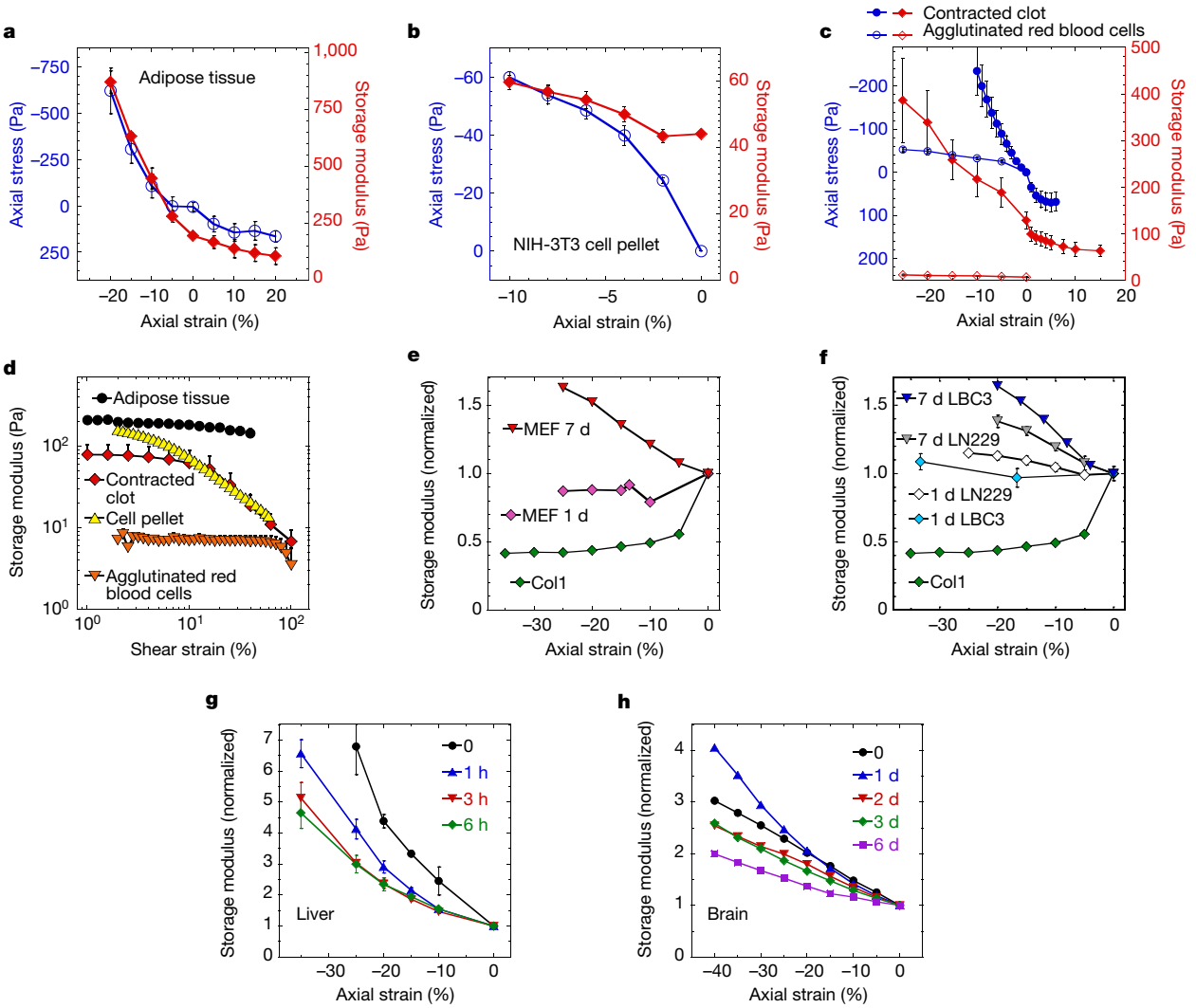

Fig. 2 | Effect of dense cell packing on multiaxial mechanics. a–**c**, Axial stress and shear storage modulus as a function of axial strain for adipose tissue (**a**), pellets of NIH-3T3 fibroblasts (**b**) and contracted blood clots and concanavalin-A-agglutinated RBC clots (**c**). Adipose tissue and contracted clots are glued to the rheometer plates with fibrin glue. The axial stress of contracted clots is measured with an Instron tensile tester with parallel plates. **d**, Storage modulus as a function of shear strain amplitude without axial strain for blood clots, RBCs and adipose tissue. For clarity one-sided error bars are shown (one standard error). **e**, **f**, Storage modulus of collagen gels (Col1) seeded with different cell types: mouse embryonic fibroblasts (MEF; **e**) and glioma cell lines LN229 and LBC3 (**f**). The gels are measured one day and seven days after seeding, after which gels have contracted substantially. **g**, **h**, Compression stiffening of liver (**g**) and brain (**h**) tissue with increasing decellularization treatment in absence of compression. The data are the means of three biological replicates, except for contracted clots in extension ($n = 5$), collagen and collagen + LBC3 ($n = 1$) and decellularized brain ($n = 1$). For MEF cells in collagen, three biological replicates were performed but one sample is shown in the graph. Error bars are one standard error.

the fibrin network to reduce the total volume by 50%, the compression stiffening effect rises to that seen for 35% beads (Fig. 3e). Contraction of the network around the beads also eliminates shear strain stiffening of the fibrin network (Fig. 3f).

Comparison of the viscoelasticity of soft tissues, fibrous networks and colloidal systems shows that tissue-like compression stiffening arises when volume-conserving particles such as cells are enclosed at high volume fractions within networks of semi-flexible polymers, but not when either constituent forms a solid material alone or when cells are embedded in a linear elastic gel. Two different mechanisms—one based on jamming of particles and the other on restrictions to the relaxation modes of fibres—might account for this effect. Jamming is essential for solidification of two-dimensional cell sheets[12,13] and inferred to have a similar role in three dimensions[14,15]. This effect would inevitably arise if the cells or particles are stiffer than the surrounding matrix, and might account for the modest effects of the stiffer dextran beads at high volume fraction on the soft polyacrylamide gel (Fig. 3d). However, jamming does not explain why very soft RBCs (Supplementary Fig. 13) also produce compression stiffening in fibrin gels. Compression stiffening in networks with cells or particles also occurs at volume fractions well below the jamming threshold in three dimensions (64%)[16], and we do not see the typical rheological footprint of a jammed system (Supplementary Figs. 18, 19). Lissajous–Bowditch plots used to characterize nonlinear mechanical response (Supplementary Fig. 20) reveal strain stiffening of fibrin networks at high shear strains even at large particle density, an effect not predicted by jamming.

To elucidate the mechanism of compression stiffening, tissue is modelled as a composite with (incompressible) cells embedded in a fibrous ECM[17] (see Supplementary Information). For simplicity, we distribute the cells on a face-centred-cubic (f.c.c.) lattice as shown in Fig. 4a, Supplementary Fig. 21. When the tissue is compressed, the cells expand in the directions perpendicular to the loading axis to conserve volume, causing tensile strains in the surrounding ECM (Fig. 4a). The magnitude of the tensile strain decays with distance from the cells (Fig. 4d). If the tissue is densely populated with cells, the strain

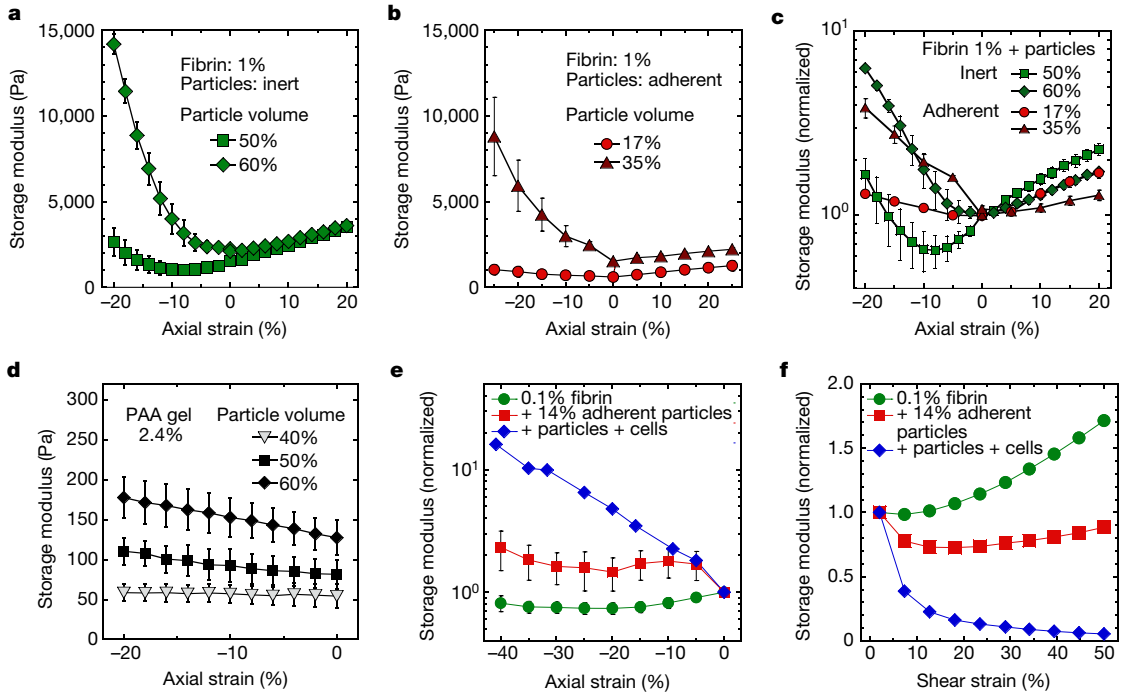

Fig. 3 | Multiaxial mechanics of networks with embedded particles. **a**, Storage modulus as a function of axial strain for 10 mg ml^{-1} fibrin networks with inert dextran beads embedded at an initial bead volume of 50% and 60% (mean of four biological replicates ± standard error). **b**, Storage modulus as a function of axial strain for 10 mg ml^{-1} fibrin networks with adherent dextran beads embedded at an initial bead volume of 17% and 35% (mean of three biological replicates ± standard error). **c**, Normalized storage moduli of all fibrin–bead composites, each sample is normalized to the storage modulus at 0% axial strain. **d**, Storage modulus as a function of axial strain for PAA networks made of 2.4% acrylamide and 0.09% bis-acrylamide cross-linker with dextran beads embedded at an initial bead volume of 40%–60%. The mean of three biological replicates ± standard error is shown. **e**, **f**, Storage modulus of 0.1% fibrin, fibrin + 14% adherent beads and fibrin + adherent beads + fibroblast cells ($n = 1$) as a function of axial strain (**e**) and as a function of shear strain (**f**).

in the ECM does not vanish, resulting in a large fraction of the ECM in tension (Fig. 4d). The stretched ECM confines expansion of the cells, leading to intracellular fluid pressure (Supplementary Fig. 23), which balances the applied compressive load. Simultaneously, owing to the alignment of extracellular fibres with the tensile principal strains, the stiffness of the ECM increases sharply (Fig. 4c). As a consequence, it becomes increasingly difficult to compress the tissue (Supplementary Fig. 26). The effect of torsional shear applied after compression is studied by considering a simple shear applied to the plane parallel to the axis of torsion, as shown in Fig. 4b. On that plane, the shear load further increases the tensile principal strain induced by compression (Supplementary Fig. 22). Because the fibrous network stiffens with increasing tensile strain, the shear stiffness of tissues increases with compression (Fig. 4e). Consistent with experiments, our model also finds that the compression stiffening of tissues requires a strain-stiffening ECM (Supplementary Fig. 28).

When a tissue is stretched, the sign of the stress near the cells becomes opposite to that observed during compression (Fig. 4a). The cells shrink in the directions perpendicular to the loading axis, causing a compressive strain in the surrounding matrix (Fig. 4c). Because the fibrous matrix cannot resist compression, negligible pressure is developed in the cells (Supplementary Fig. 23). This effectively blocks the transmission of tensile stress from the cells to the matrix. At low cell density, tension is developed in the axial loading direction and fibres align along the tensile axis, stiffening the matrix in that direction. Similarly to the fibrous material without cells, the shear modulus increases with the axial tensile deformation (Fig. 4d). When the ECM is densely populated with cells (Fig. 4d), the development of stresses directly above or below the cells is due to the generation of shear stress in what we call a 'ligament' (red dashed box), leaving a large fraction of the matrix unstrained (black dashed box). Essentially, the tensile load applied to the tissue is resisted by a small portion of the matrix that wraps around the cells (Fig. 4d). This part of the matrix is curved along the length of the cell and behaves like crimped structures[18], which straighten upon loading in tension (Supplementary Fig. 25); the crimps do not stiffen considerably before they become straight. Moreover, as the cell density increases, the volume fraction of the strained matrix decreases and its influence on tissue stiffness becomes negligible (Supplementary Fig. 24). As a result, the tissue Young's modulus does not increase substantially in tension (Supplementary Fig. 26). When the tissue is further loaded in shear deformation, the matrix is stretched in the direction 45° relative to the axis of tension. The tissue shear modulus is largely determined by the soft unstrained matrix that connects the ligaments in series (Supplementary Fig. 27). This mechanism keeps the tissue shear modulus from increasing in tension.

Increasing particle density in both experiment and simulation suppresses stiffening of fibre networks in extension but does not completely eliminate it, as is observed in some real tissues. These results suggest that other factors also contribute to tissue response. For example, our model predicts that stresses at the cell–matrix junctions are tensile in extension and can potentially dissociate cell–matrix bonds, which reduce compressional stiffening, as shown by previous studies[2]. Tissue cells are non-spherical and their volume fraction exceeds what can be packed in a fibre network in vitro. The theoretical model predicts that stiffening in extension decreases with increasing particle density and tends to zero at the close-packing limit of spheres. These minor differences are dependent on tissue type and are fully consistent with the generic features of bead–fibre network models that explain how the response of fibre networks to compression and extension is reversed as volume-conserving objects are placed within them to form materials with rheology similar to that of real tissues.

The work presented here shows the importance of high cell volume fractions as a major determinant of whole-tissue mechanics, but the main stress-bearing elements are the fibres of the ECM, which dominate the shear modulus. Understanding the viscoelastic behaviour of these composite materials can help to identify mechanisms by which

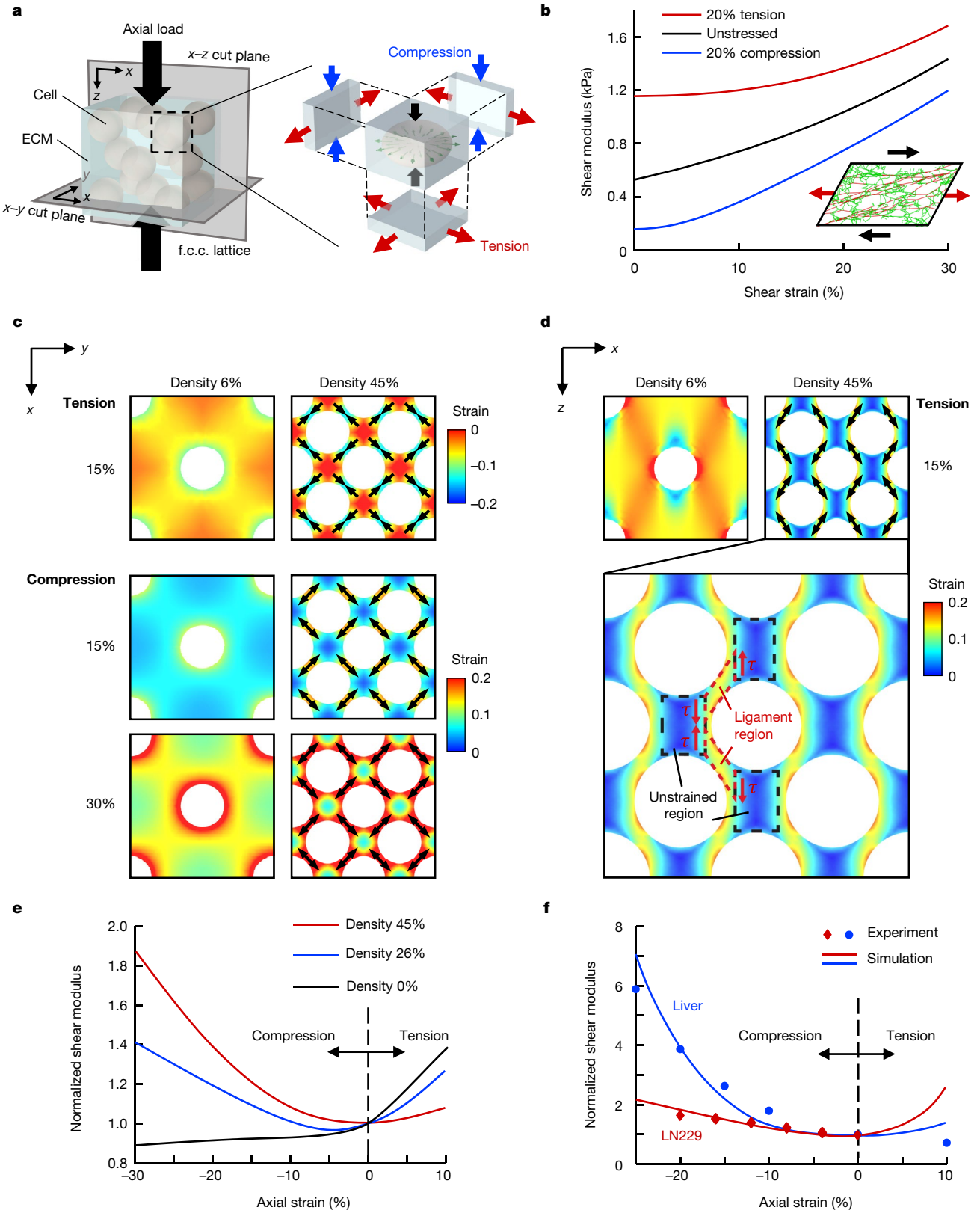

Fig. 4 | Theoretical model of fibre networks with volume-conserving inclusions. a, Model of the tissue where cells are distributed on an f.c.c. lattice. For any single cell, the stress state (blue and red arrows) in the ECM under axial compression is shown schematically. The top and bottom faces of this cube are in biaxial tension, whereas on the sides the strain is tensile (compressive) orthogonal to (along) the axis of compression. **b**, Shear modulus of the fibrous collagen network versus shear strain. The shear modulus is calculated after −20%, 0 or 20% uniaxial strain is applied to the network. The aligned fibres are marked in red. **c**, Largest principal strain in the ECM on the *x*–*y* cut plane shown in **a** when the tissue is under 15% tensile, 15% compressive and 30% compressive load. Owing to the expansion (shrinkage) of the cell in the directions perpendicular to the compressive (tensile) axial loading, the principal strain of the largest magnitude is tensile (compressive) around the cell on the *x*–*y* cut plane. The principal strain directions are shown by black arrows. **d**, Largest principal strain in the ECM on the *x*–*z* cut plane defined in **a** under 15% tensile load. τ denotes the shear stress transmitted from the 'ligament' to the unstiffened regions. **e**, Normalized shear modulus of the tissue under different levels of axial strain, calculated by the numerical model. Increasing cell density leads to more compression stiffening and less tension stiffening. **f**, Fitting of the computational model to the shear modulus of the liver tissue (cell density 72%) and the collagen gel with LN229 cells (cell density 26%).

tissue stiffness is altered in disease and to determine how this change in mechanical microenvironment leads to cellular dysfunction.

Online content

Any methods, additional references, Nature Research reporting summaries, source data, statements of data availability and associated accession codes are available at https://doi.org/10.1038/s41586-019-1516-5.

Received: 31 October 2016; Accepted: 24 June 2019;
Published online 28 August 2019.

1. Mihai, L. A., Chin, L., Janmey, P. A. & Goriely, A. A comparison of hyperelastic constitutive models applicable to brain and fat tissues. *J. R. Soc. Interface* **12**, 20150486 (2015).
2. Perepelyuk, M. et al. Normal and fibrotic rat livers demonstrate shear strain softening and compression stiffening: a model for soft tissue mechanics. *PLoS ONE* **11**, e0146588 (2016).
3. Pogoda, K. et al. Compression stiffening of brain and its effect on mechanosensing by glioma cells. *New J. Phys.* **16**, 075002 (2014).
4. Mihai, L. A., Budday, S., Holzapfel, G. A., Kuhl, E. & Goriely, A. A family of hyperelastic models for human brain tissue. *J. Mech. Phys. Solids* **106**, 60–79 (2017).
5. Budday, S. et al. Mechanical characterization of human brain tissue. *Acta Biomater.* **48**, 319–340 (2017).
6. Vahabi, M. et al. Elasticity of fibrous networks under uniaxial prestress. *Soft Matter* **12**, 5050–5060 (2016).
7. van Oosten, A. S. et al. Uncoupling shear and uniaxial elastic moduli of semiflexible biopolymer networks: compression-softening and stretch-stiffening. *Sci. Rep.* **6**, 19270 (2016).
8. Shah, J. V. & Janmey, P. A. Strain hardening of fibrin gels and plasma clots. *Rheol. Acta* **36**, 262–268 (1997).
9. Boucher, Y., Baxter, L. T. & Jain, R. K. Interstitial pressure gradients in tissue-isolated and subcutaneous tumors: implications for therapy. *Cancer Res.* **50**, 4478–4484 (1990).
10. Wyss, H. M. et al. Biophysical properties of normal and diseased renal glomeruli. *Am. J. Physiol. Cell Physiol.* **300**, C397–C405 (2011).
11. Millonig, G. et al. Liver stiffness is directly influenced by central venous pressure. *J. Hepatol.* **52**, 206–210 (2010).
12. Park, J. A. et al. Unjamming and cell shape in the asthmatic airway epithelium. *Nat. Mater.* **14**, 1040–1048 (2015).
13. Angelini, T. E. et al. Glass-like dynamics of collective cell migration. *Proc. Natl Acad. Sci. USA* **108**, 4714–4719 (2011).
14. Bi, D., Yang, X., Marchetti, M. C. & Manning, M. L. Motility-driven glass and jamming transitions in biological tissues. *Phys. Rev. X* **6**, 021011 (2016).
15. Schötz, E.-M., Lanio, M., Talbot, J. A. & Manning, M. L. Glassy dynamics in three-dimensional embryonic tissues. *J. R. Soc. Interface* **10**, 20130726 (2013).
16. Bernal, J. & Mason, J. Packing of spheres: coordination of randomly packed spheres. *Nature* **188**, 910–911 (1960).
17. Wang, H., Abhilash, A., Chen, C. S., Wells, R. G. & Shenoy, V. B. Long-range force transmission in fibrous matrices enabled by tension-driven alignment of fibers. *Biophys. J.* **107**, 2592–2603 (2014).
18. Freed, A. D. & Doehring, T. C. Elastic model for crimped collagen fibrils. *J. Biomech. Eng.* **127**, 587–593 (2005).

Acknowledgements We acknowledge R. Wells and M. Perepelyuk for collection of rat blood, S. Diamond and R. Li for surplus blood products and D. Iwamoto for reading the manuscript. This work was supported by NIH R01GM09697, NIH U54-CA193417, EB017753 and NSF-DMR-1120901 (to P.A.J., L.C., A.E.P., K.P., K.C. and A.S.G.v.O.), by the NSF Center for Engineering Mechanobiology (CMMI-154857) through grants NSF MRSEC/DMR-1720530 R01CA232256 and U01CA202177 (X.C. and V.B.S.), by a Fulbright Science and Technology Award (A.S.G.v.O.) and by Prins Bernhard Cultuurfonds-Kuitse Fonds (A.S.G.v.O.). K.P. acknowledges partial support from the National Science Center, Poland under grant number UMO2017/26/D/ST4/00997 and from the Polish-American Fulbright Commission.

Reviewer information *Nature* thanks Jasna Brujic, Ellen Kuhl and the other, anonymous, reviewer(s) for their contribution to the peer review of this work.

Author contributions A.S.G.v.O. and P.A.J. designed the experiments. A.S.G.v.O. performed the experiments that gave the data presented in Figs. 1b–g (except the adipose tissue data), 2b, d, 3a, c, f and Supplementary Figs. 2–9, 12–16, 18–20. L.C. performed the experiments that gave the results shown in Figs. 1b, c (adipose tissue data), 2a, g and Supplementary Figs. 1, 7–9, 11. K.P. obtained the data in Fig. 2f, h and Supplementary Figs. 10, 11. P.A.J., K.C. and A.E.P. provided the results in Figs. 2e, 3e, f and Supplementary Figs. 10, 11, 14, 17. V.B.S. and X.C. designed the computational model. X.C. generated the computational data. All authors contributed to the manuscript preparation.

Competing interests The authors declare no competing interests.

Additional information
Supplementary information is available for this paper at https://doi.org/10.1038/s41586-019-1516-5.
Reprints and permissions information is available at http://www.nature.com/reprints.
Correspondence and requests for materials should be addressed to V.B.S. or P.A.J.
Publisher's note: Springer Nature remains neutral with regard to jurisdictional claims in published maps and institutional affiliations.

METHODS

Human blood collection. Surplus whole blood was obtained from blood draws conducted in accordance with all appropriate guidelines and regulations and with approval of the Institutional Review Board at the University of Pennsylvania (protocol 805305). Human blood was drawn with informed consent from healthy volunteers.

Whole blood clots. Human blood was collected in the absence of anti-coagulant and immediately placed between the rheometer plates. For some samples, blebbistatin was added to the blood at 5 μg ml^{-1} (17 μM). Axial stress during polymerization of native whole clots was 72 ± 3 Pa, and ~1 Pa in blebbistatin-treated clots or purified fibrin. The blood samples were allowed to polymerize between the plates for 1.5 h at 37 °C and were surrounded with PBS-$Ca^{2+}Mg^{2+}$ after ~10 min of initial polymerization to prevent drying.

Agglutinated RBC clots. RBCs were extracted by centrifugation from whole blood drawn in K_2EDTA. The RBCs were washed three times in PBS-$Ca^{2+}Mg^{2+}$. Concanavalin A from Jack bean (L7647, Sigma) was added to a dilute RBC suspension (~5% RBC volume), with 2 mM Mn^{2+} added to the solution. The dilute RBC suspension was allowed to agglutinate for 15 min at room temperature, after which the suspension was centrifuged for 15 min at 2,000*g*. The resulting pellet (clot) was transferred to the rheometer plates and surrounded by PBS-$Ca^{2+}Mg^{2+}$ with 2 mM Mn^{2+}.

Fibrin networks. Fibrin networks were prepared similar to previously published protocols[16,19,20]. In brief, fibrinogen isolated from human plasma (CalBioChem, EMD Millipore) was dissolved in T7 buffer (50 mM Tris, 150 mM NaCl, pH 7.4). Thrombin isolated from salmon plasma (SeaRun Holdings) was diluted in ddH_2O at 1,000 units per millimetre (U ml^{-1}). To prepare fibrin networks, fibrinogen, thrombin, 1× T7 buffer and $CaCl_2$ solution were combined to yield 2 mg ml^{-1} fibrinogen, 30 mM Ca^{2+} and 2 U ml^{-1} thrombin, allowed to polymerize between the rheometer plates for 1.5–2 h at 37 °C, and then surrounded with T7 buffer.

Fibroblast pellets. NIH-3T3 fibroblasts (American Type Culture Collection (ATCC)) were cultured in 1× concentrated Dulbecco's modified Eagle medium (DMEM; ATCC) supplemented with 10% fetal bovine serum (FBS; ATCC), 1% penicillin–streptomycin (Life Technologies) and 0.1% Fungizone (Life Technologies). For every measurement, cells were detached with 0.25% trypsin-EDTA solution (Life Technologies) and spun down in two steps: the first step was for 10 min at 120*g* and the second step was for 20 min at 2,200*g*. The resulting pellet was placed between the rheometer plates and surrounded with growth medium to prevent drying.

To qualitatively check cell viability after rheometric testing, 10 μl cell suspension was replated in regular growth medium for 2 days (Supplementary Fig. 29).

Animal tissue collection. All blood samples and adipose tissues were collected from animals euthanized for the purpose of other studies performed in accordance with the guidelines of the National Institutes of Health for care and use of laboratory animals and were approved by the Institutional Animal Care and Use Committee at the University of Pennsylvania.

Mouse epididymal adipose, liver and lung tissues were obtained from adult wild-type C57BL/6 males that were at least 27 weeks old; rat liver tissue was obtained from adult male Sprague Dawley rats; and bovine spinal cord and brain were isolated from tissue received from a local abattoir. All samples were stored on ice in PBS-soaked gauze until testing, which occurred within four hours of death. Samples were cut into 8 mm diameter, or 20 mm diameter disks in the case of brain, using a stainless steel punch. To avoid slipping during shear and tensional deformation, fibrin glue was used to adhere the sample to the rheometer plates. Fibrin gel was prepared by mixing 5 μl of 28-mg ml salmon fibrinogen with 10 units of thrombin directly onto the lower rheometer plate; the sample was placed on top and subsequently fibrin gel was also applied to the upper surface of the tissue. The top plate was lowered until contact was made, as determined by the application of approximately 1*g* of normal force. The sample was surrounded by PBS to prevent drying of the tissue during testing.

Tissue decellularization. Rat liver and bovine brain were subjected to decellularization following modifications of published protocols[2]. In brief, samples were placed into a decellularization solution (liver, 2% Triton X-100, 0.1% SDS in PBS at 37 °C; brain, 0.1% SDS, 1% penicillin–streptomycin in PBS at 4 °C), allowed to shake for various lengths of time and then rinsed with PBS for 15 min before rheometry.

Contracted clots. Contracted clots were prepared from blood collected from 300–350 g Sprague-Dawley rats (Charles River Laboratories) after dissection of the vena cava without the use of anti-coagulant. The blood was immediately transferred to a tissue culture dish, resulting after 2 h in disk-shaped contracted clots that were removed for rheological testing. To prevent slipping, contracted clots were glued with fibrin glue similarly to the adipose tissue. The samples were surrounded by PBS-$Ca^{2+}Mg^{2+}$ to prevent drying.

Cells in collagen gel. The LN229 cell line was obtained from ATCC (CRL2611). Cells were grown in DMEM (Gibco) supplemented with 10% FBS (Gibco) and 100 U ml^{-1} penicillin and 100 μM streptomycin (Sigma-Aldrich).

Three-dimensional collagen gels were prepared from the following ingredients: a stock solution of 4.13 mg ml^{-1} collagen I (BD Bioscience), DMEM 5× concentrated solution (Gibco) and DMEM 1× concentrated solution (Gibco), FBS (Gibco) and 0.1 M NaOH. Cells were counted, pelleted and resuspended in DMEM, followed by addition of FBS, NaOH and collagen I. All of the ingredients were kept on ice to prevent early gelation. Collagen gel mixture was transferred into 12-well plates (1 ml of the gel mixture per well) and immediately placed inside a humidified incubator at 37 °C and 5% CO_2. Gels were allowed to sit for at least 60 min and immersed in fresh DMEM after gelation was complete. The initial density of glioma cells was adjusted to 200,000 cells per millilitre. The shear moduli of the three-dimensional collagen gels were determined on day 1 and day 7 post-preparation using a Kinexus rheometer (Malvern Instruments) equipped with 20 mm diameter parallel plates.

Fibrin networks with embedded beads. The fibrinogen described for fibrin networks was used. Beads made from cross-linked dextran (Sephadex G-25 medium, GE Health Sciences) were swollen with ddH_2O to accomplish 92% swelling. The volume needed for 92% swelling was extrapolated from the amount of water needed for 100% swelling. The 100% swelling was determined by allowing pre-weighed beads to swell for 12 h in excess amounts of ddH_2O. The suspension was centrifuged at 2,200*g* for 30 min, and the weights of the beads and excess water were determined. Fully swollen, the dextran beads had 50–150 μm diameter and an exclusion limit of 80 kDa (hence fibrinogen is excluded). For rheometry, fibrinogen, T7 buffer, $CaCl_2$ solution, thrombin and distilled water were mixed together and then added to a bead solution to yield a 10-mg ml^{-1} fibrin network in a 1× T7 buffer with 0.5 units thrombin per millilitre of sample and a 50% or 60% volume of beads, assuming continued swelling of 92% swollen beads when placed in excess buffer. Samples were polymerized between the rheometer plates for 90 min at 25 °C and surrounded by T7 buffer.

Adherent beads (SP Sephadex C-25, GE Health Sciences) were used similarly with the following modifications: fibrinogen from salmon plasma was used (SeaRun Holdings) and beads were swollen to 100% (v/v) in 1× T7 buffer.

PAA gels with embedded dextran beads. A solution of 8% acrylamide and 0.3% bis-acrylamide cross-linker (BioRad) in ddH_2O was mixed with 10% ammonium persulfate and TEMED to initiate polymerization, after which it was quickly mixed with pre-swollen G-25 medium dextran beads and ddH_2O to yield a network with 2.4% acrylamide, 0.09% bis-acrylamide, 0.2% APS, 0.3% TEMED and 40%, 50%, 60% or 70% beads. The networks were polymerized in a non-adhesive container with a thickness of 1–2 mm for 45 min at room temperature. After full polymerization, samples were cut to size, transferred to the rheometer plates and surrounded by ddH_2O.

Rheometry. A strain-controlled rotational RFS3 rheometer (TA Instruments) with parallel plates was used. For whole clots, a plate of 50 mm diameter was used with a 400-μm gap. For adipose tissue, a plate of 8 mm diameter was used. The top plate was lowered until contact was made, as determined by the application of 1*g* of normal force. Contracted clots, RBC clots, fibrin networks (with and without particles) and PAA networks with particles were tested with a plate of 25 mm diameter and a gap of 1–2 mm. A Peltier device incorporated into the bottom plate was used to control the sample temperature at 37 °C for blood and cell clots and 25 °C for composites of networks and beads as well as tissue. Samples were kept hydrated with the appropriate buffer during the experiments. The shear modulus was measured by applying a low oscillatory shear strain of 1%–2% at a frequency of 10 rad s^{-1}. Axial strain was applied by changing the gap between the plates. Samples were subjected to small step-wise axial strains, between which the samples were allowed to relax. An Instron 5569 tensile tester with parallel platens was used to measure axial stresses of contracted clots.

Reporting summary. Further information on research design is available in the Nature Research Reporting Summary linked to this paper.

Data availability

The data that support the findings of this study are available from the corresponding authors upon reasonable request.

Code availability

The computational code developed in this work is included as Supplementary Code. The source code is covered under the GNU general public license, version 2.0 (GPL-2.0).

19. Berryman, J. G. Random close packing of hard spheres and disks. *Phys. Rev. A* **27**, 1053–1061 (1983).
20. Scott, G. & Kilgour, D. The density of random close packing of spheres. *J. Phys. D* **2**, 863–866 (1969).

nature research

Corresponding author(s): Anne van Oosten, Paul Janmey, Vivek Shenoy

Last updated by author(s): 2019-4-4

Reporting Summary

Nature Research wishes to improve the reproducibility of the work that we publish. This form provides structure for consistency and transparency in reporting. For further information on Nature Research policies, see Authors & Referees and the Editorial Policy Checklist.

Statistics

For all statistical analyses, confirm that the following items are present in the figure legend, table legend, main text, or Methods section.

n/a	Confirmed
☐	☒ The exact sample size (*n*) for each experimental group/condition, given as a discrete number and unit of measurement
☐	☒ A statement on whether measurements were taken from distinct samples or whether the same sample was measured repeatedly
☒	☐ The statistical test(s) used AND whether they are one- or two-sided *Only common tests should be described solely by name; describe more complex techniques in the Methods section.*
☒	☐ A description of all covariates tested
☒	☐ A description of any assumptions or corrections, such as tests of normality and adjustment for multiple comparisons
☒	☐ A full description of the statistical parameters including central tendency (e.g. means) or other basic estimates (e.g. regression coefficient) AND variation (e.g. standard deviation) or associated estimates of uncertainty (e.g. confidence intervals)
☒	☐ For null hypothesis testing, the test statistic (e.g. *F*, *t*, *r*) with confidence intervals, effect sizes, degrees of freedom and *P* value noted *Give P values as exact values whenever suitable.*
☒	☐ For Bayesian analysis, information on the choice of priors and Markov chain Monte Carlo settings
☒	☐ For hierarchical and complex designs, identification of the appropriate level for tests and full reporting of outcomes
☒	☐ Estimates of effect sizes (e.g. Cohen's *d*, Pearson's *r*), indicating how they were calculated

Our web collection on statistics for biologists contains articles on many of the points above.

Software and code

Policy information about availability of computer code

Data collection	COMSOL5.3 Matlab 2017b
Data analysis	ImageJ 1.51h imageJ.nih.gov Matlab R2015B and Matlab 2017b

For manuscripts utilizing custom algorithms or software that are central to the research but not yet described in published literature, software must be made available to editors/reviewers. We strongly encourage code deposition in a community repository (e.g. GitHub). See the Nature Research guidelines for submitting code & software for further information.

Data

Policy information about availability of data

All manuscripts must include a data availability statement. This statement should provide the following information, where applicable:

- Accession codes, unique identifiers, or web links for publicly available datasets
- A list of figures that have associated raw data
- A description of any restrictions on data availability

Requests for data can be addressed to corresponding authors

Field-specific reporting

Please select the one below that is the best fit for your research. If you are not sure, read the appropriate sections before making your selection.

☒ Life sciences ☐ Behavioural & social sciences ☐ Ecological, evolutionary & environmental sciences

For a reference copy of the document with all sections, see nature.com/documents/nr-reporting-summary-flat.pdf

Life sciences study design

All studies must disclose on these points even when the disclosure is negative.

Sample size	size calculation was not performed, standard practice was to test at least 3 distinct samples per condition, in certain cases this was not possible due to availability of samples
Data exclusions	no data were excluded
Replication	In most cases at least three distinct samples were tested. In certain cases this was not possible, in those cases there could be made a comparison was made between different tissues or species.
Randomization	Not relevant
Blinding	Not relevant

Reporting for specific materials, systems and methods

We require information from authors about some types of materials, experimental systems and methods used in many studies. Here, indicate whether each material, system or method listed is relevant to your study. If you are not sure if a list item applies to your research, read the appropriate section before selecting a response.

Materials & experimental systems

n/a	Involved in the study
☒	☐ Antibodies
☐	☒ Eukaryotic cell lines
☒	☐ Palaeontology
☐	☒ Animals and other organisms
☐	☒ Human research participants
☒	☐ Clinical data

Methods

n/a	Involved in the study
☒	☐ ChIP-seq
☒	☐ Flow cytometry
☒	☐ MRI-based neuroimaging

Eukaryotic cell lines

Policy information about cell lines

Cell line source(s)	NIH3T3, LN229 from American Type Culture Collection (ATCC, Manassas, VA) LBC3 cells were isolated from human GBM tissue as previously described in Walsh, E. M., Kim, R., Del Valle, L., Weaver, M., Sheffield, J., Lazarovici, P., & Marcinkiewicz, C. (2012). Importance of interaction between nerve growth factor and α9β1 integrin in glial tumor angiogenesis. Neuro-oncology, 14(7), 890-901 Mouse embryo fibroblasts (mEFs) were provided by J. Ericsson (Åbo Akademi University, Turku, Finland)
Authentication	ATCC authenticates cell lines
Mycoplasma contamination	LN229 were tested for mycoplasma contamination, other cell lines were not. Mycoplasma testing is not critical since this research focusses on the effect of cell traction on fibrous networks, and not cell signaling etc
Commonly misidentified lines (See ICLAC register)	No cell lines used are in ICLAC register

Animals and other organisms

Policy information about studies involving animals; ARRIVE guidelines recommended for reporting animal research

Laboratory animals	Mouse; adult wild type C57BL/6 males that were at least 27 weeks old Rat: adult male Sprague Dawley rats, Charles River Laboratories, Malvern, PA

Wild animals	Study did not involve wild animals
Field-collected samples	Bovine spinal cord and brain were isolated from tissue received from a local slaughterhouse, tissue was transported at 4C and kept moist by keeping it in PBS soaked gauze
Ethics oversight	National Institutes of Health guidelines for care and use of laboratory animals Institutional Animal Care and Use Committee at the University of Pennsylvania.

Note that full information on the approval of the study protocol must also be provided in the manuscript.

Human research participants

Policy information about studies involving human research participants

Population characteristics	Participants were only selected at the criteria that they were currently healthy and not having taken any medication in the 2 weeks prior to the blood draw
Recruitment	Participants were volunteers from primarily the student body of the engineering faculty at the university. In these experiments there is no risk of bias due to the recruitment method or incentives
Ethics oversight	Internal Review Board at the University of Pennsylvania (protocol 805305)

Note that full information on the approval of the study protocol must also be provided in the manuscript.